JOURNAL OF GEOPHYSICAL RESEARCH, VOL. 114, F01006, doi:10.1029/2007JF000941, 2009

Dimensions of dry snow slab avalanches from field measurements

D. M. McClung[1]

Received 3 November 2007; revised 29 April 2008; accepted 23 September 2008; published 23 January 2009.

[1] Dry slab avalanches release by a sequence of propagating fractures. In this paper, I provide field measurements of the important length parameters resulting from fractures for hundreds fallen slabs including depth, length, and width. The field data show wide variations in these parameters. Probability plots of all dimensions (length, width, and depth) suggest they approximately obey log normal probability density functions. Given slab dimensions, two applications are considered on the basis of the field data. These applications are: (1) Estimates of total fracture energy consumed around the perimeter of the slab are given, where it is presumed fracture is mostly mode I, and along the base (weak layer) of the slab, where shear fracture (mode II and III) is expected. For average characteristic dimensions, the analysis suggests that energy consumed on the perimeter is somewhat less than in the weak layer. Even though fracture energy around the perimeter is expected to be higher than in the weak layer, the larger area fractured in shear at the base of the slab compared to area fractured in tension around the perimeter results in a comparable amount of total energy needed around the perimeter. (2) Approximate estimates of avalanche mass for average characteristic dimensions based on slab depth D (the only length possibly known prior to avalanching) are made. The mass is considered related to destructive potential and simple guidelines are given to estimate mass in relation to D with validation by considering concurrent size and estimates of D by mountain guides.

Citation: McClung, D. M. (2009), Dimensions of dry snow slab avalanches from field measurements, *J. Geophys. Res.*, *114*, F01006, doi:10.1029/2007JF000941.

1. Introduction

[2] Field observations and measurements show conclusively that propagating shear fractures (mode II and mode III) within a thin weak layer underneath a thicker, stronger snow slab are responsible for dry snow slab release [*McClung*, 1979, 1981]. Prior to avalanche release of the fundamental lengths B, L, and D (slab width, length, and thickness, respectively), the only one that can be estimated prior to avalanche release is depth to the weak layer, D since the weak layer can be found from snow profiles and field tests.

[3] Field measurements show that the ratio of slab width (B) to length (L) is, on average, approximately $B/L \approx O(1)$ [*Brown et al.*, 1972; *Jamieson and Johnston*, 1990, 1992; *McClung and Schaerer*, 2006]. The fractures determining the ratio B/L are formed entirely on the slab perimeter. These include tensile fracture at the crown along a distance and tensile or shear fractures along the sides (or flanks). One reason to expect that the ratio B/L should be of order 1 is that the fracture energy for slab material, whether in shear or tension, is expected to be similar [*McClung*, 2007a].

[4] Field observations show that the shear fracture propagates upslope from the initiation point underneath a slab of thickness D for a distance L after which tensile fracture initiates through the body of the slab at nearly a right angle to the weak layer [*Perla*, 1971; *McClung*, 1979, 1981]. Field measurements and observations show that the ratio of slab length to thickness $L/D \gg 1$ but wide variations in the ratio are observed. I suggest that the value of the ratio (L/D) is linked to the ratio of slab tensile fracture energy (G_I) to weak layer shear fracture energy (G_{II}). *McClung* [2007a] determined that, on average, the ratio is $10 < (G_I/G_{II}) < 16$ with a range between about 1–300, derived from field estimates hundreds of dry snow slabs.

[5] A fundamental question in regard to fracture energy is the relationship between the energy needed to entirely fracture the weak layer compared to the energy required to fracture the slab around its perimeter. In this paper, simple estimates are derived for the ratio of energy consumed around the perimeter to that within the slab base. Given the avalanche dimensions presented in this paper combined with a simple model for slab geometry and suggested values for G_I/G_{II}, it is possible to estimate the ratio of energy to form fractures on the perimeter to the weak layer. For average or median values of slab dimensions, the ratio is found to be less than one but approaching or exceeding one for extreme cases.

[6] The field data presented below (Table 1) show that, on average, the ratio of slab length to thickness is $L/D \approx 100$

[1]Department of Geography, University of British Columbia, Vancouver, British Columbia, Canada.

0148-0227/09/2007JF000941$09.00

Table 1. Descriptive Statistics for Measured and Estimated Length Ratios

Ratio	Number of Avalanches	Median	Range	Comments
B/*L*	26	2.1	1–5	Unconfined avalanches
B/*L*	63	1.2	0.25–5	Mix of confined and unconfined avalanches
B/*D*	130	113	6–875	Mix of confined and unconfined avalanches
B/*D*	3470	85	3–2000	Data are estimated, not measured; confined and unconfined avalanches; value of *B* is estimated as minimum width
L/*D*	63	100	17–750	Mix of confined and unconfined avalanches

and the ratio of width to length is $B/D \approx 1$ with wide variations in both ratios. Given these ratios, it is possible to estimate avalanche volume for simple models. Since avalanche volume is related to mass and destructive potential, it is suggested that a knowledge of *D* prior to avalanche release can help to estimate expected avalanche mass. In this paper, avalanche mass is estimated on the basis of simple modelling and field measurements, as a function of *D*. The mass is then related to a five part scale for size on the basis of destructive potential used in the Canada and the United States [*McClung and Schaerer*, 2006, p. 322] and verification is provided by use of size estimates and measurements of *D* provided by mountain guides.

2. Length Dimensions of Dry Snow Slabs From Field Measurements and Field Estimates

[7] In this section, I report length dimensions from fallen snow slabs measured in the field and similar data for which the dimensions are estimated but not precisely measured. The three important length scales are defined according to Figure 1. The length *D* slab is depth, measured or calculated, through the slab perpendicular to the weak layer. There is some lack of precision in estimates for *D* since in the field, observations show that slab depth varies around the crown where tensile fracture has taken place. For this paper, values of *D* will be taken to be the mean crown thickness. The parameter *D* is a fundamental scaling parameter in relating fracture mechanical size effects [*Bažant et al.*, 2003] for slab initiation.

[8] The parameter *L* is taken to be the mean distance between the crown and the lower portion of the slab, called the stauchwall. Length data for slabs are much more scarce than crown height or width because the lower boundary (stauchwall) is often obscured by downslope slab motion in the initial stages of motion. The parameter *B* is taken to be the mean distance between the flanks. As with *D*, the values of *B* and *L* are normally single representative measurements rather than mean values taken from multiple estimates.

[9] Field observations show that there is no precise form for the outline of the fracture pattern from a slab avalanche taken as a plan view. *Perla* [1971] suggested on the basis of a small number of slabs, that the crown is not straight in the majority of cases but instead, it takes a curved form. Sometimes the plan view form is nearly elliptical (Figure 1a) with hardly any visible straight flanks. In this paper, I will consider two simple forms for the fracture pattern in plan view: rectangular and elliptical as illustrated in Figure 1. Figure 2a contains a photo of a slab with approximately elliptical shape but there are others with nearly rectangular shape with length greater than width relatively unconfined with respect to terrain features. Figure 2b shows avalanches with length greater than width and dimensions affected by terrain features.

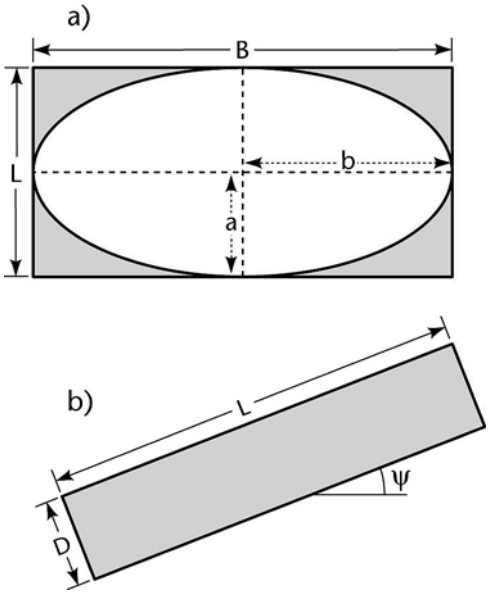

Figure 1. Schematic of slab geometry for either (a) elliptical or (b) rectangular shape. The three length scales *D*, *B*, and *L* are shown. For the elliptical model, the semiminor and semimajor axes are $a = L/2$ and $b = B/2$, respectively.

Figure 2a. Slab avalanche cut free by fractures. In this case, the slab geometry is approximately elliptical and the slab geometry does not appear affected by terrain features (unconfined) and slab width is greater than slab length. Photo courtesy of T. Salway.

Figure 2b. Two slabs with length longer than width. Terrain features affect the dimensions in these cases (confined). Photo courtesy of A. Roch.

2.1. Slab Length Parameters From Field Measurements

[10] Figure 3 contains a probability plot for values of D measured for 191 slab avalanches. The ordinate is a logarithmic scale so that the plot suggests that values of D follow a log normal probability density function. The range of values is from 0.1 to 4.2 m with median 0.66 m and mean of the log normal distribution is 0.67 ± 0.07 m. The wide range of values approximates the expected range for most applications. Figure 3 is for avalanches with a mix of triggers (natural, explosives, skier triggering) and similar patterns are found for data sets for one trigger only (skier triggering, natural). I conclude that the length parameter D approximately follows a log normal probability density function regardless of trigger.

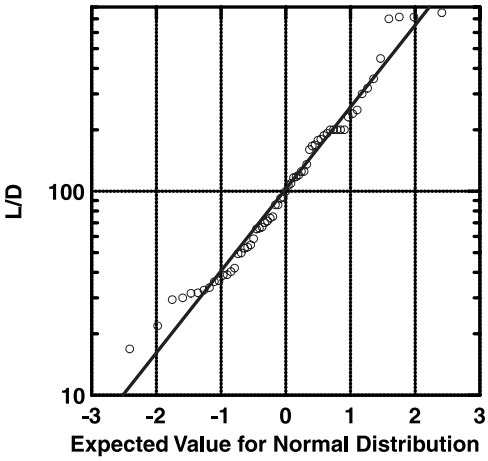

Figure 4. Probability plot of the ratio L/D from 63 slab avalanches similar to Figure 3.

[11] Figure 4 contains a probability plot of the ratio L/D from 63 slab avalanche measurements. Similar to Figure 3, the plot suggests that the ratio follows a log normal probability density function. The median value for L/D is close to 100 with the mean of the log normal distribution being 103 but the range has nearly 3 orders of magnitude from approximately 10–1000.

[12] Figure 5 contains a probability plot of the ratio B/D from field measurements of 130 avalanches. Conclusions similar to Figure 4 follow: log normal dependence with nearly 3 orders of magnitude range. The median value is 113 and mean of the log normal distribution is also 113 but

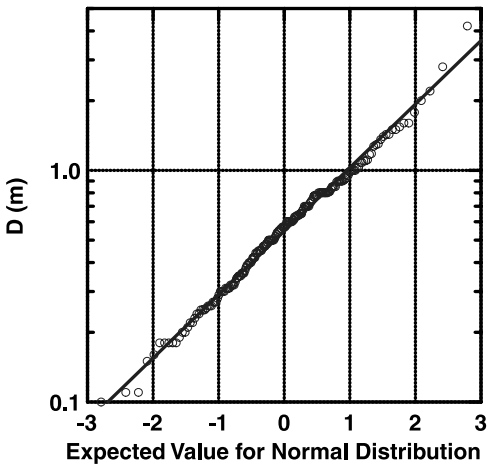

Figure 3. Probablity plot for values of D for 191 avalanches. The plot suggests D follows a log normal probability density function.

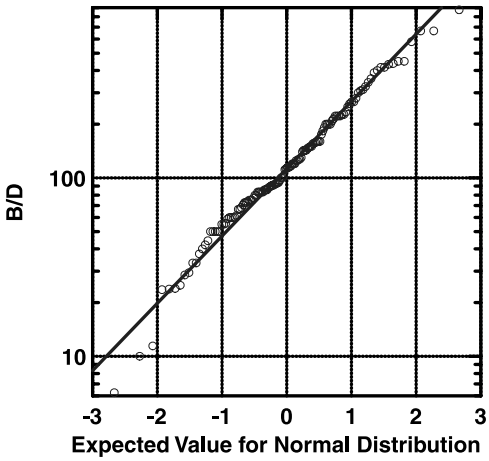

Figure 5. Probability plot of the ratio B/D for 130 slab avalanches. The data are from terrain which is a mix of unconfined and confined.

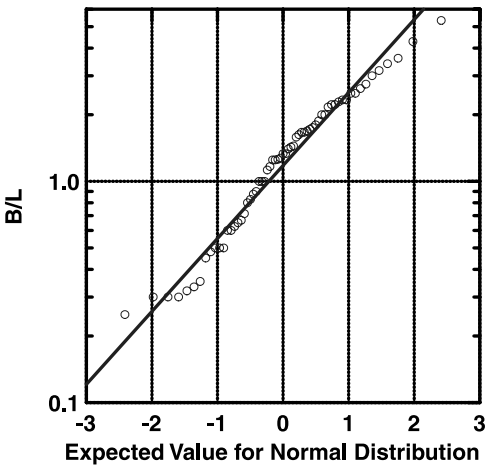

Figure 6. Probability plot of the ratio B/L for 63 slab avalanches. The data are from terrain which is a mix of unconfined and confined.

similar to Figure 5, nearly 3 orders of magnitude range for the ratio are evident.

[13] Figure 7 contains a probability plot of measurements for B/L from a limited data set where all the avalanches are unconfined by terrain features. Again, the ordinate is logarithmic so the plot suggests a log normal probability density function is followed. However, only 26 data points are plotted so firm conclusions are not available. The plot shows that the ratio varies from just over 1 to about 6 with a median near 2. The plot is congruent with the suggestion by *Brown et al.* [1972] that slabs are wider than they are long. Figure 6 contains a plot of B/L for 63 avalanches similar to Figure 7. These data are for slabs which may be confined or unconfined so that some slabs may be influenced by terrain features. The mean of the log normal distribution is 1.2 for this data set. The plot shows that slabs may have width as low as 20% of the length.

[14] There are examples of slabs with length greater than width when gully walls or other terrain features prevent lateral extension of fractures as in Figure 2b see also [*McClung and Schaerer*, 2006, p. 94]. Thus, terrain features can have significant effects on slab dimensions. The mean of the log normal distribution and median sample values from Figure 7 are both 2.1, which suggests that, on average, unconfined slabs are about twice as wide as they are long.

[15] From Figures 4 and 5 the mean value of the log normal distribution of B/D (113) is about that for L/D (100) for data from the same set. These values suggest that B and L, on average, are comparable, given a value of D, at least for this larger set of slabs, which contains mixed confined and unconfined terrain. *Schweizer and Lütschg* [2001] analyzed 69 human triggered avalanches (confined and unconfined). They found a median value $B/L = 0.8$ which confirms that B and L are comparable.

[16] An important factor is that an initial slab can expand laterally or downslope to engulf other slabs which can produce widths and lengths which are unreasonably large for single slabs [*McClung and Schaerer*, 2006]. Unfortunately, it is not possible to isolate those cases from the data in this paper but they are important to explain the upper limit of the distributions of the ratios L/D and B/D in the data presented, as well as the range of 3 orders of magnitude.

2.2. Dimensions From Fallen Avalanches Estimated But Not Measured

[17] In this section, I report data from fallen avalanches for values of D, B, and B/D for fallen avalanches with part of the data estimated by field observers rather than measured. The values of D may be regarded as more accurate than the values of B since the slab depth is often estimated from known depth to the weak layer whereas B is normally estimated by simple, visual observations. The observations have been recorded by the mountain guides of Canadian Mountain Holidays who are generally skilled field observers. The data consist of more than 3000 slabs and the results confirm some of the conclusions of section 2.1.

[18] Figure 8 contains a probability plot of values for D (2758 slabs) and Figure 9 contains a similar plot for B/D

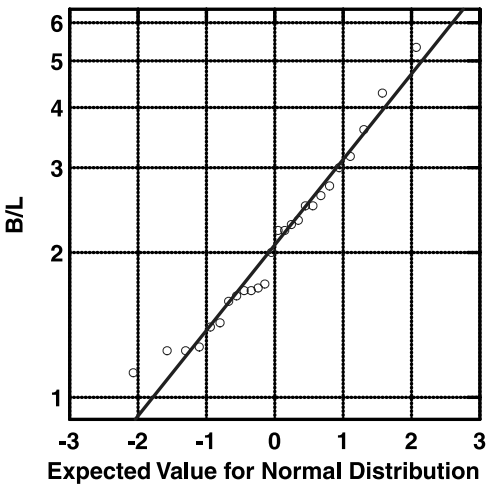

Figure 7. Probability plot of the ratio B/L for 26 slab avalanches. The data are from terrain which is unconfined. The data are contained in Figure 6.

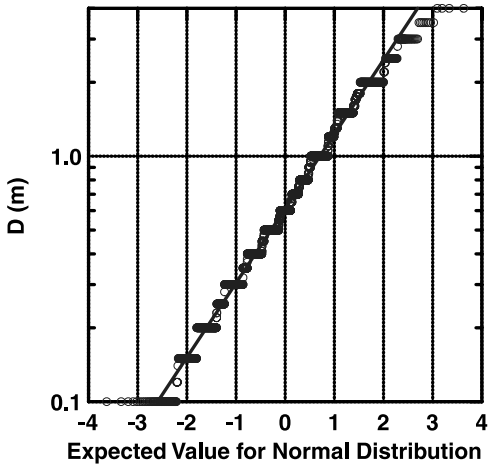

Figure 8. Probablity plot for values of D for 3258 slab avalanches. The plot suggests D follows a log normal probability density function. The data are estimated, not measured.

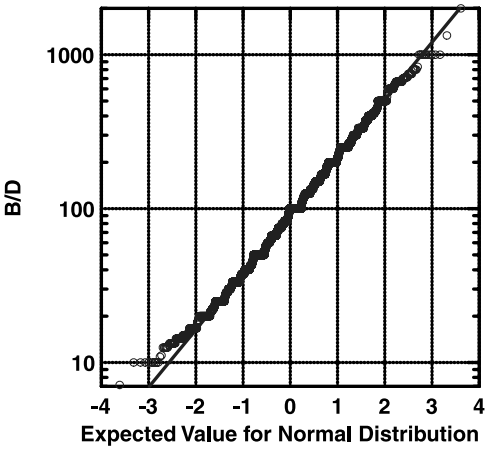

Figure 9. Probability plot of the ratio B/D for 3470 slab avalanches similar to Figure 5. The data are estimated, not measured.

(2758 slabs). For Figure 9, the median value from both sample statistics and the mean value for the log normal distribution are both 100. Again, both plots suggest that log normal dependence is a good approximation for the distributions.

[19] Table 1 contains a summary of the descriptive statistics for the ratios B/L, B/D, and L/D for all the measured and estimated lengths from field data. The data are measured unless otherwise noted. The sample medians are close to the means of the log normal distributions for the ratios.

[20] From Table 1, I conclude that the median values both L/D and B/D are about 100 for a mix of confined and unconfined avalanches. From measurements, the median value of B/L is about 1 for a mix of confined and unconfined avalanches. However, for the small set of unconfined avalanches, the median value is about 2. The values L/D = 100, B/L = 1 (mix of confined and unconfined avalanches), and B/L = 2 (unconfined avalanches) are used in the applications below to estimate fracture energy consumed and mass related to destructive potential.

3. Simple Geometrical Model Representing Snow Slab Area

[21] In this section, I consider a simple geometrical model for the snow slab. Figure 2a, shows a typical snow slab geometry. In this case, a simple elliptical shape might approximate the outline of the slab in plan view with a semiminor axis $a = L/2$ and semimajor axis $b = B/2$ and the ratio being $b/a \approx 3$. If the case of elliptical geometry chosen, the flanks would have a theoretical length of zero. For the other extreme, with rectangular geometry, the flanks would have length equal to L. Thus, these two extremes are chosen as the geometrical model below for calculations of slab area, volume and length on the slab perimeter. Figure 1 shows the simple slab geometry model used in the applications below. The case shown is for $b = 2a$ or $B = 2L$ as might be expected for average conditions for unconfined avalanches.

[22] On the basis of the data in section 2, and the schematic in Figure 1, the area of the base is given by

$$\begin{aligned} A_{\text{base}} &= \pi \frac{BL}{4} (\rightarrow \text{ellipse}) \\ A_{\text{base}} &= BL (\rightarrow \text{rectangle}). \end{aligned} \tag{1}$$

The area of the perimeter is given by

$$\begin{aligned} A_{\text{perim}} &= 2\pi D \sqrt{\frac{L^2 + B^2}{8}} (\rightarrow \text{ellipse}) \\ A_{\text{perim}} &= (2B + 2L) D (\rightarrow \text{rectangle}). \end{aligned} \tag{2}$$

In equation (2), the circumference of an ellipse is approximated by

$$C_{\text{ellipse}} = 4a \int_0^{\frac{\pi}{2}} \sqrt{1 - k^2 \sin(\phi)}\, d\phi \approx 2\pi \sqrt{\frac{a^2 + b^2}{2}},$$
$$k = \sqrt{1 - \left(\frac{a}{b}\right)^2}. \tag{3}$$

In the applications below, equations (1) and (2) are applied for the following values and limits: L/D = 100, B/L = 2(unconfined), and B/L = 1(confined/unconfined). Field observations (e.g., Figure 2a) show that D can vary considerably around the crown, particularly for large avalanches. Slab taper [*Perla*, 1977] is an important factor. Given these observations, only approximate estimates are available for the applications below.

[23] From equations (1) and (2), on average, the ratio of basal area to perimeter area is typically between 25 and 35 using L/D = 100 as a median value with D constant all along the perimeter. This is only a rough estimate since effects such as slab taper are not accounted for and, due to wide variations in L/D, variations in the area ratio may be expected.

4. Approximate Ratio of Fracture Energy Consumed on the Slab Perimeter to That Along the Bed Surface

[24] In this section, I consider the ratio between the total energy needed to produce tensile and shear fracture along the perimeter of slab avalanches to the total energy needed to produce shear fracture over the entire area within the weak layer of slabs. In this section, median values are used for the dimension ratios and fracture energies of the weak layer and slab to yield rough values of the ratio of energy consumed around the slab perimeter to that within the weak layer. In Appendix A, I consider the energy ratio based on the ranges of length ratios from the slab measurements and fracture energies suggested by *McClung* [2007a]. In this section, only the median values of fracture energy and slab dimensions are used to estimate the energy ratio (slab perimeter vs. slab base) but Appendix A is added to suggest that wide variations may be expected in the ratio.

[25] Fracture at the base of slabs in the fragile weak layer is suggested to happen by a combination of mode II (in plane) and mode III (antiplane) shear fracture [*McClung*, 1981; *Bažant et al.*, 2003; *McClung*, 2007a]. For the simple application here, the approximation is made that weak layer

mode II fracture energy is approximately equal to the mode III fracture energy $G_{II} \approx G_{III}$ where the fracture energy is the energy required to produce a unit area of fracture surface (J/m^2).

[26] Fracture around the perimeter through the slab is assumed to occur in either tension or shear. Shear fractures do not readily propagate in homogeneous materials. Instead, normally a relatively this weak layer is needed. Thus, for slab material tensile fracture is favored. *McClung* [2007a] provided information to suggest that the values of fracture energy (G_I and G_{II}) are approximately equivalent for the material making up the slab. Thus, I approximate the fracture energy around the perimeter as G_I (mode I) at all locations even though shear fracture through the slab may occur at some places around the perimeter.

[27] Using the rectangular geometrical model above, the ratio of energy needed to the perimeter compared to the energy needed on the base is

$$\frac{E_{\text{perim}}}{E_{\text{base}}} = \frac{G_I}{G_{II}}\left(\frac{4D}{L}\right) = 0.4 - 0.6(\rightarrow B = L)$$
$$\frac{E_{\text{perim}}}{E_{\text{base}}} = \frac{G_I}{G_{II}}\left(\frac{3D}{L}\right) = 0.3 - 0.5(\rightarrow B = 2L), \quad (4)$$

where the median value of $L/D = 100$ from Table 1 and the median value of $10 < G_I/G_{II} < 16$. Since the ratio G_I/G_{II} follows a log normal distribution when calculated from field data [*McClung*, 2007a], there is theoretical support for the form of equation (4) if the ratios (L/D and G_I/G_{II}) can be assumed to be independent. In that case, the log normal distribution has the property that the median of the product of log normal distributions (L/D and G_I/G_{II}) is given by the product of the medians of the individual distributions [*Benjamin and Cornell*, 1970, p. 269].

[28] Similar calculations for the elliptical model give

$$\frac{E_{\text{perim}}}{E_{\text{base}}} = \frac{G_I}{G_{II}}\left(\frac{4D}{L}\right) = 0.4 - 0.6(\rightarrow B = L)$$
$$\frac{E_{\text{perim}}}{E_{\text{base}}} = \frac{G_I}{G_{II}}\sqrt{10}\left(\frac{D}{L}\right) = 0.3 - 0.5(\rightarrow B = 2L). \quad (5)$$

I conclude that, given the approximations, the energy needed for fracture around the perimeter is about 30–60% of that needed to fracture the weak layer and base. Taking into account slab taper, suggests that these values may be an upper limit since slab taper could reduce the area around the perimeter. The uncertainties by approximating weak layer fracture as all in mode II and perimeter fracture as all in mode I produce unknown errors on the results. The estimates from equation (5) are derived from median values of the ratios G_I/G_{II} [*McClung*, 2007a] and D/L derived from field measurements of slab avalanches. Since there are wide variations in both ratios, wide variations in $E_{\text{perim}}/E_{\text{base}}$ are possible (Appendix A). The discussion in Appendix A is important since the data for the ratios which are used to estimate $E_{\text{perim}}/E_{\text{base}}$ come from independent data sets but physically the ratios may not be independent for individual avalanches.

[29] Slab displacement downhill following weak layer shear provides the energy to drive the shear fractures within the weak layer and at the base. The energy per unit area provided by downhill slip of magnitude $\bar{\delta}$ is given by $\rho g D \sin\psi(\bar{\delta})$ where ρ, g, and ψ are mean slab density, magnitude of acceleration due to gravity and slope angle (Figure 1) respectively. The mean characteristic displacement during strain softening, shear fracture of alpine snow is $\bar{\delta} \approx 0.1$ mm [*McClung*, 2007b; D. M. McClung, Dry snow slab quasi-brittle initiation and verification from field tests, paper submitted to *Journal of Geophyical Research*, 2008]. For typical values ($\rho = 200$ kg/m^3, $D = 0.5$ m, and $\psi = 35°$) calculation gives about 0.06 J/m^2 which is 3–4 times the median value of G_{II} estimated for slab avalanches by *McClung* [2007a]. Thus, one might expect, on average, that downhill release of gravitational energy can easily provide the energy to fracture the weak layer.

[30] *Perla* [1971] studied the fracture patterns of dry slab avalanches from a limited data set and he concluded that in the majority of cases the crown fracture is curved. Field experience shows that this is true in some cases (Figure 2a). Figure 10 contains schematics of forces associated with down slope slab movement which could produce tension fracture along the curved portions of both the crown and stauchwall. At the crown (scenario 1 of Figure 10), tension fracture in at the center of the slab may become curved as it advances laterally and downslope slab motion is influenced by friction at the sides. The same pattern of tensile fractures is observed near the sides of glaciers [*Paterson*, 1994] where downslope motion is resisted by friction at the edge of the glacier.

[31] Field observations suggest that the stauchwall is the last fracture surface to be formed [*McClung and Schaerer*, 2006]. Thus, the slab is already in motion when the stauchwall is being formed with compressive force resisting the downslope motion. Resolution of these two forces (scenario 2 of Figure 10), gives a pair of forces in compression and another in tension which could produce a curved stauchwall. For both the crown and the stauchwall, tensile fracture is expected perpendicular to the resolved maximum principal tensile stress or highest value of tensile stress. It would be difficult, if not impossible, to calculate the maximum principal stress under the dynamic conditions expected. Thus, Figure 10 may be regarded as one possible explanation of the curved fracture surfaces which are seen in some avalanches.

5. Estimates of Mass and Destructive Potential From Slab Measurements as a Function of *D*

[32] The only slab dimension that can be estimated prior to avalanche release to an avalanche forecaster or a back country traveller in avalanche terrain is the depth, D, to the weak layer. The sections above suggest that, on average, the mass of avalanches might be estimated for the simple geometrical model since relations between L, B and D are provided by field data. The Canadian and American system [*McClung and Schaerer*, 2006, p. 322] for sizing avalanches is based on destructive potential of which one important component is the estimated mass. In this section, I provide simple estimates of avalanche mass as a function of D. This enables guidelines for values of D for mass estimates in the size systems based on destructive potential. I will use the

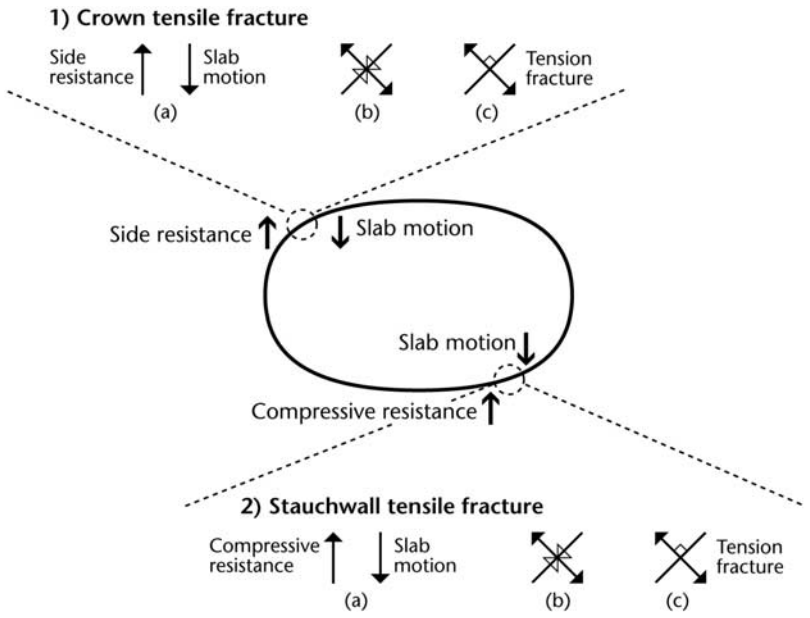

Figure 10. Schematic showing possible evolution of curved fracture surfaces by mode I (tensile) fracture at the crown (scenario 1) and stauchwall (scenario 2). At the crown (scenario 1), downhill slab force combined with side friction force may produce tensile fracture perpendicular to the resolved tensile force. At the stauchwall (scenario 2), bottom compressive resistance and downhill slab thrust force could combine to produce a curved tension fracture similar to the crown.

parameters in section 4 above and the geometrical model of section 3 and Figure 1 to provide simple estimates.

[33] In order to estimate the mass M as a function of D, a simple relationship between mean slab density and depth is needed. For the data in Figure 3 (191 avalanches), a nonlinear least squares regression was performed to yield a relationship between mean slab density ρ, and depth

$$\rho = 225D^{0.24} \text{ kg/m}^3. \tag{6}$$

In equation (6), the t statistics for both of the constants are highly significant with α values <0.001 but there is considerable scatter (R^2 = 0.18 where R is the Pearson correlation coefficient). For the data set, the median value of D is 0.57 m with a range 0.1–4.2 m.

[34] For the rectangular model, the mass is given by $M = \rho BLD$. The expressions for mass in tonnes are then given by (with L/D = 100)

$$\begin{matrix} M = 2250D^{3.24} (\rightarrow B = L) \\ M = 4500D^{3.24} (\rightarrow B = 2L) \end{matrix} \text{ tonnes.} \tag{7}$$

For the elliptical model, the expressions are

$$\begin{matrix} M = 2250\left(\frac{\pi}{4}\right)D^{3.24} (\rightarrow B = L) \\ M = 2250\left(\frac{\pi}{2}\right)D^{3.24} (\rightarrow B = 2L) \end{matrix} \text{ tonnes.} \tag{8}$$

Solving for D gives a relation of the form

$$D = \left(\frac{M}{225C_0}\right)^{0.31} \text{m}, \tag{9}$$

where C_0 is a constant depending the geometrical model. For the rectangular model, $C_0 = 10(\rightarrow B = L)$ and $20(\rightarrow B = 2L)$ and for the elliptical model, $C_0 = 2.5\pi(\rightarrow B = L)$ and $5\pi(\rightarrow B = 2L)$. Table 2 contains the order of magnitude size classification system used in Canada and USA [*McClung and Schaerer*, 2006] along with the depth guidelines from equation (9) based the limits with the different values of C_0.

[35] The size guidelines (D) for sizes 4 and 5 are given by a footnote because the estimates do not include entrainment of material which is a known feature [*Sovilla*, 2004; *Sovilla et al.*, 2006] of large avalanches. It can be expected in such cases that the total mass may be higher by almost a factor approaching 10 than the initial slab mass. Thus, for sizes 4 and 5, the depth guidelines could be overestimates even though the guidelines are for average rather than extreme cases. This may also be true for size 3 in some cases.

[36] From equation (9), an order of magnitude increase in mass yields a two fold increase in D (i.e., $10^{0.31}$ = 2.04). The depth estimates for the different sizes provide important guidelines for avalanche forecasters and back country travellers if it is remembered that they are typical values for average size (mass) and wide variations are expected. *McClung and Schaerer* [2006] suggest that a definition of acceptable risk in back country travel is that it is unacceptable to trigger a size 2 avalanche. The guideline in Table 2 suggests that typical slab depths could be expected in the range 30–40 cm for size 2, which may aid in decisions. *McClung and Schaerer* [2006] suggested 30 cm of new snow as an important threshold for a danger signal for backcountry travel.

[37] The slab depth estimates in Table 2 are theoretical estimates based upon median avalanche lengths estimated from field measurements and simple geometrical modelling. The mountain guides of Canadian Mountain Holidays have

Table 2. Avalanche Size Classification System From Canada and United States With Depth Guidelines for Different Sizes of Avalanche Based on Mass

Size	Description	Typical Mass (t)	Typical Path Length (m)	Typical Impact Pressure (kPa)	Typical Slab Depth D (m)
1	Relatively harmless to people	<10	10	1	0.15–0.20
2	Could bury, injure, or kill a person	100	100	10	0.30–0.40
3	Could bury a car or destroy a small building or a few trees	1000	1000	100	0.60–0.80
4	Could destroy a railway car, large truck, several buildings, or a forest with area up to 4 hectares	10,000	2000	500	1.3–1.7[a]
5	Largest snow avalanches known; could destroy a village or forest of 40 hectares	100,000	3000	1000	2.6–3.5[a]

[a]Sizes with mass expected to be affected by entrainment.

estimated both slab depth D and avalanche size according to the Canadian avalanche size system in the first 4 columns of Table 2. In Table 3, I summarize the estimated avalanche size (median of D) and the theoretical values from Table 2. Mountain guides in Canada use half sizes for which there is no definition in the size system. For Table 3, half sizes were rounded up to the next size class, for example, size 2.5 was counted as size 3 in order to fit the data into the size classes of the size system.

[38] From Table 3, the depth guidelines are close to, but somewhat below, the medians of depths estimated by guides. Typically, the median values from the guides estimates are within 20 centimeters of the upper limits of the guidelines. This comparison suggests that, from the perspective of making decisions, the depth guidelines are slightly conservative which is desirable for applications. It must be remarked that guides use the other columns of Table 2 including the text description, as well as mass guidelines, for estimating size or destructive potential. If only those avalanches estimated to be in even size numbers (1, 2, 3, and 4) are used, then the median depths and No. of avalanches are changed respectively to: size 1 (0.35 m, 312), size 2 (0.60 m, 739), size 3 (1.2 m, 357), size 4 (2.0 m, 34). The estimates are virtually identical for sizes 1, 2, and 3 with a slight difference for size 4.

6. Limitations and Approximations

[39] Many approximations are used to arrive at the approximate results in the applications in this paper. They are as follows:

[40] 1. The slab height D is taken as the mean value all along the perimeter of the slab from a single measurement taken at the crown. Field observations show that slab thickness can vary not only all along the crown but all along the slab perimeter as well. Slab taper, noted by *Perla* [1977], can occur along the crown as well as on the flanks. In addition, very few examples exist whereby people have taken enough measurements to accurately determine mean or median crown height. The values used in this paper are approximate estimates of mean crown thickness represented by single measurements.

[41] 2. For most of the examples, there is no information on how slab width, B, might be affected by terrain features or forest cover. Furthermore, most estimates of B are single measurements which are taken to represent the mean width. There are no data to accurately estimate the mean or median width for any of the cases. The same comments apply to the values of L. The values of L are supposed to represent mean values but, like B and D, they represent single measurements measured at a position which is approximately the mean value by inspection.

[42] 3. The two simple geometrical models used (rectangular and elliptical) represent extremes for maximum value of flank length: equal to L (rectangular) and minimum flank length: equal to zero (elliptical). The two median ratios of B/L (1 and 2) used in the applications are determined from limited data sets of 63 and 26 avalanches respectively. The ratios may be subject to revision when larger data sets become available.

[43] 4. Data for the values of L are limited because, in most cases, the stauchwall is covered or destroyed after the slab breaks free and moves down the slope. In this paper, only 63 values of L are used. The median of the ratio L/D = 100 is used with both limits (B/L = 1 or 2) to estimate area or volume. Thus, for example, if B/L = 1 then the basal area is half that for B/L = 2 using the rectangular model. There is not enough information about slab geometry with the data set to show how realistic such approximations are.

[44] 5. In order to estimate the energy consumed for fracture through and around the perimeter of the slab, the value of mode I fracture energy G_I was used on the crown, stauchwall and flanks. Sometimes the flanks are straight (see the rectangular model of Figure 1b) which suggests that flank fracture may have been in shear (mode II). I suggested [*McClung*, 2007a] from simple shear experiments that the slab fracture energy for mode II for homogeneous snow is comparable to mode I and this has been suggested by experimental results that shear and tensile fracture toughness are comparable for homogeneous samples [*Schweizer et al.*, 2004]. Normally, mode II fracture is not expected in

Table 3. Median Value of D and Avalanche Size Estimated by Mountain Guides and Theoretical Depth Guidelines for the Sizes From Table 2

Size	Number of Avalanches	Median of Depths Estimated (m)	Depth Guidelines From Table 2 (m)
1	312	0.35	0.15–0.20
2	1197	0.50	0.30–0.40
3	1088	1.00	0.60–0.80
4	158	1.5	1.3–1.7

homogeneous materials. Instead, a layered structure is needed such as the weak layer fracture for dry snow slab avalanches. Figure 10 contains the suggestion that the curved fractures sometimes observed on the crown and stauchwall may consist of mode I fracture. Another similar approximation used in section 4 is that mode III fracture energy is comparable to mode II fracture energy for avalanche weak layers. I expect these values should be comparable but there are no measurements or theoretical estimates of weak layer mode III fracture energy to confirm this. In addition, it is not known what fraction of weak layer fracture is mode II or mode III.

[45] 6. The applications in this paper are derived from empirical relations based on field data. Equations (4) and (5) should be taken to provide empirical rather than theoretical results. It has to be emphasized that the product of ratios $(G_I/G_{II})(D/L)$ is derived from different databases. The conclusions from equations (4) and (5), should not be extrapolated beyond those derived from the product of the medians of these ratios.

7. Summary and Conclusions

[46] The following conclusions result from field measurements, field observations, and simple theoretical considerations subject to the limitations listed in section 6:

[47] 1. On average, the ratio of slab length to thickness is L/D; 100, the ratio of slab width to thickness is B/D; 100 and the median ratio of width to length is $B/L \approx 1.2$ for confined and unconfined avalanches with many cases having $B/L < 1$. For unconfined avalanches, *Brown et al.* [1972] predicted that the ratio B/L should be greater than one in all cases. This suggestion fits with the median of the data for unconfined avalanches in this paper for which the median value of B/L for is 2.1.

[48] 2. The field data show that all the key length scales (B, L, and D) are approximately log normally distributed as well as the ratios and products of these. The log normal distribution has a multiplicative property [*Benjamin and Cornell*, 1970] so it is expected that ratios and products should be log normal. Some of the probability plots of the ratios show a lack of fit at the lower or upper bounds of the data. The log normal character is only a rough approximation. Goodness of fit tests may indicate other distributions as candidates for use with the data, particularly if the shape of the distribution is important in applications. All plots involving D show wide variations in the ratios and all length scales exhibit ranges of nearly 3 orders of magnitude.

[49] 3. The curved crown tensile fracture line (modelled as elliptical here) is probably due to shear friction resistance on the flanks combined with the downhill force of the slab caused by gravitational energy release as shear fractures propagate up and across slope (Figure 10).

[50] 4. The curved bottom (stauchwall) fracture line which is seen in some cases is probably due mostly to tension fracture as a result of downhill slab motion thrust (after crown tensile fracture), combined with compressive support at the lower boundary of the slab as viewed in plan (Figure 10). The explanation here, as well as that for point 3 above, may be regarded as one possible explanation of curved surfaces but there is no conclusive proof offered here.

[51] 5. For the data and approximations in this paper, on average, the energy consumed by tensile fracture around the slab perimeter is somewhat less than the shear fracture energy consumed in the weak layer at the base of the slab. Wide variations in slab dimensions and fracture energies prevent a general statement of this suggestion. Appendix A contains a simple analysis employing some of the variations and I suggest that no general statement is possible. Limitation 6 above also addresses this point.

[52] 6. Available slab gravitational energy released by downhill slab motion should exceed energy consumed in creation of basal (weak layer) fracture surface by a considerable margin.

[53] 7. For constant D, the slab dimension data suggest that, on average, the basal area fractured in shear is more than 25 times the area fractured around the perimeter in tension or shear. If slab taper is taken into account, this value will increase since measurements of D are from the crown where slab thickness is normally maximum.

[54] 8. On the basis of comparison of median slab depths estimated by guides, the depth guidelines calculated from avalanche data seem reasonable for the size categories in the Canadian avalanche size system. The maximum depth from the depth guidelines is within 20 centimeters of the median of depths estimated by guides in each size class (Table 3).

Appendix A: Ratio of Energy Consumed on the Slab Perimeter to That at the Base Considering Variations in Fracture Energy and the Ratio *L/D*

[55] From section 4, the energy ratio around the slab perimeter to that at the base may be represented by

$$\frac{E_{\text{perim}}}{E_{\text{base}}} = C\left(\frac{G_I}{G_{II}}\right)\left(\frac{D}{L}\right). \tag{A1}$$

where C is a constant with value between 3 and 4. From *McClung* [2007a], the ratio G_I/G_{II} takes values between approximately 1 and 300 with a median about 10. The avalanche data (Figure 3) suggest that the ratio L/D varies between about 30 and 800 with a median value about 100. Given that the ratio G_I/G_{II} follows a log normal distribution [*McClung*, 2007a] when calculated from avalanche data and that the ratio L/D follows a log normal distribution, it is reasonable to expect the product will follow a log normal distribution. The product of the medians (the mean of the log normal distributions) then gives 0.1 or a rough estimate of the energy ratio, on average, as 0.3–0.4 as suggested in section 4. Pairing the extremes of the data is equivalent to the assumption that there is no correlation between the fracture energy and length ratios. Repeating the calculations by pairing the highest value of G_I/G_{II} (300) with the lowest value of L/D (30) and vice versa gives a range for the energy ratio in equation (A1) of 0.004–30. Given that the distribution of the product should be log normal, most of the data would be expected to fall in the range for the energy ratio between 0.01 and 10 (3 orders of magnitude) with center of the distribution falling somewhere between 0.1 and 1.

[56] Field observations suggest that the two ratios (G_I/G_{II} and L/D) are not always independent. Stiff, tough, thick slabs tend to allow shear fracture propagation over long

distances before tensile fracture through the crown results in avalanche release [*McClung and Schaerer*, 2006, p. 93]. As the shear fracture propagates, tensile stresses are built in the slab. The simplest model is to assume that the avalanche release is imminent once the tensile fracture toughness is reached in a small region at the base of the slab just above the weak layer after propagating a distance L. Higher slab density at the base, associated with thick slabs, gives higher tensile fracture toughness requiring longer propagation distances to accumulate higher tensile stresses in order to reach the tensile fracture toughness. The process is explained by *McClung and Schweizer* [2006].

[57] The prominent feature of dynamic mode II propagation in the weak layer is the stress drop, q, behind the fracture process zone following propagation [*Freund*, 1990]. As the shear fracture propagates over a distance L, a simple one-dimensional model suggests tensile stresses build approximately as $q(L/D)$ [*Palmer and Rice*, 1973; *McClung*, 1981] until tensile fracture toughness is reached in a small boundary layer at the bottom of the slab [*McClung and Schweizer*, 2006]. The concepts suggest that higher tensile fracture energy (or higher tensile fracture toughness) in the slab should be associated with longer propagation distance. The propagation distances from fallen avalanches, $L/D > 30$, are much larger than the ratio of L/D needed for shear fracture initiation which is about 1 either for the size effect law of *Bažant et al.* [2003] or the verification by hundreds of field tests [*Gauthier*, 2007]. Thus, I suggest that the length ratio L/D enters the problem from the tensile stress (or stress concentration factor) accumulated at the bottom of the slab as the shear fracture propagates. This physical interpretation suggests that larger values of L/D should be paired with higher values of the ratio G_I/G_{II} in equation (A1) and vice versa. Applying these pairings gives the limits for $E_{\text{perim}}/E_{\text{base}}$ between $(0.5-0.375)C$ or a range of values for the energy ratio as $E_{\text{perim}}/E_{\text{base}}$ between 0.15 and 1.5, with a typical value of about 0.5 as suggested in section 4.

[58] There are many effects not accounted for in the physical model here including slab stratigraphy and dynamic effects on the shear fracture propagation. Given uncertainties in the parameters, the safest conclusion is reached by using only the average values (medians of the distributions) as in section 4. The physical picture here suggests that energy consumed on the perimeter might exceed that at the base in extreme cases but, even then, the magnitude of the ratio is of order 1. As suggested above, the opposite assumption, (that there is no correlation between G_I/G_{II} and L/D), gives a much larger range for the energy ratio but the average value for the energy ratio is still expected to be somewhat less than one which is the only claim made in this paper.

[59] The wildly varying properties of avalanche dimensions, combined with field observations, favor the first interpretation of little or no correlation between the ratios G_I/G_{II} and L/D. Spearman rank correlation of L with D for the limited data available shows positive correlation but it is not significant statistically. The weak correlation of mean slab density with slab depth in equation (6) also indicates high scatter in the avalanche data. At present, there is no database for which both ratios (G_I/G_{II} and L/D) are estimated to aid in firmer conclusions.

[60] **Acknowledgments.** This research was sponsored by Canadian Mountain Holidays and the Natural Sciences and Engineering Research Council of Canada. I am extremely grateful for the support. Data were provided by Canadian Mountain Holidays as recorded by their mountain guides. Jürg Schweizer, WSL, Swiss Federal Institute for Snow and Avalanche Research, also provided important data on slab dimensions.

References

Bažant, Z. P., G. Zi, and D. McClung (2003), Size effect law and fracture mechanics of the triggering of dry snow slab avalanches, *J. Geophys. Res.*, *108*(B2), 2119, doi:10.1029/2002JB001884.

Benjamin, J. R., and C. A. Cornell (1970), *Probability, Statistics and Decision for Civil Engineers*, 684 pp., McGraw-Hill, New York.

Brown, C. B., R. J. Evans, and E. R. LaChapelle (1972), Slab avalanching and the state of stress in fallen snow, *J. Geophys. Res.*, *78*(24), 4950–4958.

Freund, L. B. (1990), *Dynamic Fracture Mechanics*, 563 pp., Cambridge Univ. Press, Cambridge, U. K.

Gauthier, D. (2007), A practical field test for fracture propagation and arrest in weak snowpack layers in relation to slab avalanche release, Ph.D. thesis, 302 pp., Dep. of Civil Eng., Univ. of Calgary, Calgary, Alberta, Canada.

Jamieson, J. B., and C. D. Johnston (1990), The width of unconfined slab avalanches based on field measurements of slab properties, paper presented at International Snow Science Workshop, Int. Snow Sci. Workshop Comm., Bigfork, Montana, 9–13 October.

Jamieson, J. B., and C. D. Johnston (1992), A fracture-arrest model for unconfined dry slab avalanches, *Can. Geotec. J.*, *29*, 61–66.

McClung, D. M. (1979), Shear fracture precipitated by strain-softening as a mechanism of dry slab avalanche release, *J. Geophys. Res.*, *84*(B7), 3519–3526.

McClung, D. M. (1981), Fracture mechanical models of dry slab avalanche release, *J. Geophys. Res.*, *86*(B11), 10,783–10,790.

McClung, D. M. (2007a), Fracture energy applicable to dry snow slab avalanche release, *Geophys. Res. Lett.*, *34*, L02503, doi:10.1029/2006GL028238.

McClung, D. M. (2007b), Fracture properties of faceted snow, Geophys. Res. Abstr., *9*, abstract 03123.

McClung, D. M., and P. Schaerer (2006), *The Avalanche Handbook*, 3rd ed., 342 pp., Mountaineers, Seattle, Wash.

Palmer, A. C., and J. R. Rice (1973), The growth of slip surfaces in the progressive failure of over-consolidated clay, *Proc. R. Soc. London Ser. A*, *332*, 527–548.

Paterson, S. (1994), *The Physics of Glaciers*, 3rd ed., 480 pp., Elsevier, Oxford, U. K.

Perla, R. I. (1971), The slab avalanche, Ph.D. thesis, 101 pp., Dep. of Meteorol., Univ. of Utah, Salt Lake City.

Perla, R. I. (1977), Slab avalanche measurements, *Can. Geotech. J.*, *14*(2), 206–213.

Schweizer, J., and M. Lütschg (2001), Characteristics of human-triggered avalanches, *Cold Reg. Sci. Technol.*, *33*, 147–162.

Schweizer, J., G. Michot, and H. O. K. Kirchner (2004), On the fracture toughness of snow, *Ann. Glaciol.*, *38*, 1–8.

Sovilla, B. (2004), Field experiments and numerical modelling of mass entrainment and deposition processes in snow avalanches, Ph.D. dissertation, 191 pp., Swiss Fed. Inst. of Technol., Zurich, Switzerland.

Sovilla, B., P. Burlando, and P. Bartelt (2006), Field experiments and numerical modelling of mass entrainment in snow avalanches, *J. Geophys. Res.*, *111*, F03007, doi:10.1029/2005JF000391.

D. M. McClung, Department of Geography, University of British Columbia, 1984 West Mall, Vancouver, BC V6T 1Z2, Canada. (mcclung@geog.ubc.ca)